BIOCHEMISTRY
including biophysical chemistry & molecular biology

Article

pubs.acs.org/biochemistry

Analysis and Assay of Oseltamivir-Resistant Mutants of Influenza Neuraminidase via Direct Observation of Drug Unbinding and Rebinding in Simulation

Christopher J. Woods,*[,†] Maturos Malaisree,[†] Benjamin Long,[‡] Simon McIntosh-Smith,[‡] and Adrian J. Mulholland*[,†]

[†]Centre for Computational Chemistry, School of Chemistry, University of Bristol, Bristol BS8 1TS, U.K.

[‡]Department of Computer Science, University of Bristol, Bristol BS8 1TS, U.K.

Supporting Information

ABSTRACT: The emergence of influenza drug resistance is a major public health concern. The molecular basis of resistance to oseltamivir (Tamiflu) is investigated using a computational assay involving multiple 500 ns unrestrained molecular dynamics (MD) simulations of oseltamivir complexed with mutants of H1N1-2009 influenza neuraminidase. The simulations, accelerated using graphics processors (GPUs), and using a fully explicit model of water, are of sufficient length to observe multiple drug unbinding and rebinding events. Drug unbinding occurs during simulations of known oseltamivir-resistant mutants of neuraminidase. Molecular-level rationalizations of drug resistance are revealed by analysis of these unbinding trajectories, with particular emphasis on the dynamics of the mutant residues. The results indicate that MD simulations can predict weakening of binding associated with drug resistance. In addition, visualization and analysis of binding site water molecules reveal their importance in stabilizing the binding mode of the drug. Drug unbinding is accompanied by conformational changes, driven by the mutant residues, which results in flooding of a key pocket containing tightly bound water molecules. This displaces oseltamivir, allowing the tightly bound water molecules to be released into bulk. In addition to the role of water, analysis of the trajectories reveals novel behavior of the structurally important 150-loop. Motion of the loop, which can move between an open and closed conformation, is intimately associated with drug unbinding and rebinding. Opening of the loop occurs coincidentally with drug unbinding, and interactions between oseltamivir and the loop seem to aid in the repositioning of the drug back into an approximation of its original binding mode on rebinding. The similarity of oseltamivir to a transition state analogue for neuraminidase suggests that the dynamics of the loop could play an important functional role in the enzyme, with loop closing aiding in binding of the substrate and loop opening aiding the release of the product.

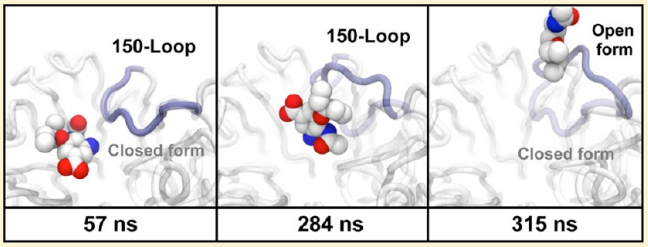

Oseltamivir is the most extensively used antiviral treatment for influenza. Oseltamivir, marketed as Tamiflu, is an orally active inhibitor of the neuraminidase protein. It has seen widespread deployment as a treatment for seasonal (e.g., H3N2), avian (H5N1), and pandemic influenza (H1N1-2009).[1−3] This success has led several governments to build up large stockpiles of oseltamivir, in preparation for possible future influenza pandemics.[2−4] However, widespread use of this drug has been linked to the emergence of resistant mutants of the virus.[5,6] This is a major concern, because, if such variants become widespread, oseltamivir could become ineffective as a treatment in a future influenza pandemic. Understanding how particular mutations of neuraminidase give rise to resistance is a key priority, both to support the development of new antiviral influenza treatments and to allow the prediction of drug-resistant mutants. Here, we study mutants of neuraminidase from H1N1-2009 pandemic influenza complexed with oseltamivir. The results support the findings of previous studies[7−10] and provide new insights into the mechanisms of unbinding and binding of oseltamivir. They indicate that molecular dynamics (MD) simulations on the time scale of hundreds of nanoseconds (made possible by the use of GPUs) can directly predict weakened drug binding and may be effective as a predictive assay for drug resistance.

BACKGROUND

There are two major subtypes of neuraminidase in human influenza, N1 and N2. The major difference between these subtypes is the flexibility of the 150-loop, which moves between an open and closed conformation.[11] While X-ray structures of both the open and closed forms of the 150-loop are known for the N1 subtype,[11,12] only closed forms of N2 have been successfully crystallized.[13,14] The role of neuraminidase during influenza viral replication is to cleave sialic acid, which is

Received: June 13, 2013
Revised: October 2, 2013
Published: October 15, 2013

   dx.doi.org/10.1021/bi400754t | *Biochemistry* 2013, 52, 8150−8164

necessary to allow the release of the newly replicated virus from infected cells.[15] Oseltamivir was designed to target neuraminidase by acting as a mimic of sialic acid. It was developed on the basis of X-ray structures of a transition state analogue of sialic acid complexed to the closed conformation of an N2 neuraminidase.[16] Despite being designed to target N2, oseltamivir is also a potent inhibitor of N1 neuraminidase, with crystal structures available showing the drug bound to both the open and closed forms.[11,12]

Oseltamivir was first published by Kim and co-workers in 1997[16] and was then approved by the U.S. Food and Drug Administration (FDA) in 1999 as the first orally available antiviral agent specifically for influenza.[17] While designed as an analogue of sialic acid, oseltamivir contains a bulky hydrophobic group that is not present in the substrate (see Figure 1).

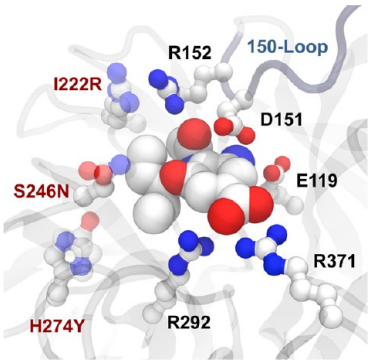

Figure 1. Oseltamivir bound in the active site of H1N1-2009 neuraminidase. Residues involved in binding the drug are shown, together with the 150-loop. The I222R, S246N, and H274Y mutations were studied. These residues are close to the hydrophobic "bulky group" of oseltamivir, with H274Y and S246N forming part of the bulky group binding pocket that is disrupted by oseltamivir binding.

The size of this bulky group requires the rearrangement of the active site residues of neuraminidase upon ligand binding.[16] Variants of neuraminidase have emerged with mutations of residues in or near this "bulky group binding pocket". One such variant involves a single mutation, substituting histidine for tyrosine at position 274 [H274Y using N2 numbering, hereafter termed HY (see Figure 1)]. This variant was one of the first N1 mutants to demonstrate significant oseltamivir resistance,[18−20] with a 327−982-fold loss of drug efficacy reported (see Table 1).[21−25]

Oseltamivir was used widely during the 2005 H5N1 "bird flu" pandemic. Use of oseltamivir was accompanied by a significant increase in the number of reports of the emergence of HY oseltamivir-resistant mutants.[18] The number of reports of this mutant increased further during the later H1N1-2009 "swine flu" pandemic, with more than 600 cases of HY resistance reported to the World Health Organization.[28]

In parallel with the widespread deployment of oseltamivir against the H1N1-2009 swine flu pandemic, several further novel mutants with high oseltamivir resistance were reported.[23,24,26] These included a single mutant of H1N1-2009 involving substitution of isoleucine with arginine at position 222 [I222R, hereafter termed IR (see Figure 1)]. This was first isolated from a child in November 2009. The child was receiving prolonged oseltamivir and zanamivir treatment to target infection from H1N1-2009 influenza. Treatment was ineffective, suggesting the IR mutation conferred resistance to both inhibitors.[24] Later experiments confirmed that the mutant exhibited mild drug resistance, with a 28−53-fold loss of efficacy versus that of the wild type (see Table 1). After the first case was found, several further reports of the IR mutant were made, either as a single mutant or coupled with the original HY mutation as a dual I222R/H274Y mutant (hereafter termed IRHY).[23,27] The double IRHY mutant was found to be extremely drug resistant, with oseltamivir measured to have a 1647−16307-fold loss of efficacy compared to that of the wild type (see Table 1).[22,23,25] This loss of binding strength was sufficient to render oseltamivir an ineffective treatment.

Table 1. Experimentally Reported Binding Affinities, Measured as IC_{50}, of Oseltamivir for Mutants of Neuraminidase, Compared to That for the Wild Type[a]

	IC_{50} (nM)		
	wild type	mutant	loss of efficacy
SN	0.45 ± 0.35	2.68 ± 0.61	6[26]
IR	0.34 ± 0.14	9.49 ± 2.19	28[27]
	0.20 ± 0.08	9.1 ± 1.2	45[24]
	0.46 ± 0.01	24.48 ± 2.12	53[25]
HY	0.25 ± 0.12	81.75 ± 30.95	327[21]
	0.26 ± 0.07	86.26 ± 30.08	375[22]
	0.25 ± 0.12	125.62 ± 37.26	502[23]
	0.20 ± 0.08	108 ± 12	540[24]
	0.46 ± 0.01	451.90 ± 26.01	982[25]
SNHY	0.45 ± 0.35	2646.81 ± 293.55	5880[26]
IRHY	0.46 ± 0.01	757.39 ± 68.65	1647[25]
	0.25 ± 0.12	3093.49 ± 44.99	12374[23]
	0.26 ± 0.07	3750.68 ± 854.94	16307[22]

[a]Loss of drug efficacy is reported as the ratio of mutant and wild-type binding strength.

In addition to the IR mutant, an oseltamivir-resistant mutant involving substitution of serine at position 246 with asparagine [S246N, hereafter termed SN (see Figure 1)] has been reported. Reports began in 2009, with an increased rate from specimens in Australia, Brunei, and Singapore from 2011.[26] The SN mutant has been measured to have only a slight (6-fold) loss of binding efficacy compared to that of the wild type (see Table 1). However, as for IR, SN has also been reported as part of a highly drug resistant dual mutant with HY. The dual S246N/H274Y mutant (hereafter termed SNHY) exhibits high levels of oseltamivir resistance, with one report suggesting a 5880-fold loss of binding efficacy compared to that of the wild type (see Table 1).[26] This decrease was sufficient to render oseltamivir an ineffective treatment of the dual SNHY mutant.

Efforts to date to understand the molecular basis of how these mutations confer oseltamivir resistance have relied on analysis of static X-ray crystal structures of oseltamivir−neuraminidase complexes,[11−13,29−34] and computational studies involving molecular dynamics and free energy calculations of oseltamivir complexed with the mutants.[7−10,35−38] These have resulted in hypotheses of mechanisms of drug resistance that point to long time scale changes in the dynamics and structure of neuraminidase but are necessarily limited by the short time scales that can be achieved by these techniques.[7−10,35−38] To unify these hypotheses, and to confirm long time scale behavior, we embarked on a series of 500 ns molecular dynamics (MD) simulations of oseltamivir complexed to the wild type and all of the aforementioned mutants of H1N1-2009 neuraminidase. These simulations were facilitated by gaining early access to the then new, 372-GPU (nVidia Tesla graphics

dx.doi.org/10.1021/bi400754t | Biochemistry 2013, 52, 8150−8164

processor) Emerald supercomputer cluster. Emerald was at the time one of the largest GPU-based clusters in Europe and allowed an order-of-magnitude increase in sampling compared to that of our previous study.[7] Here, each simulation involved 500 ns of unrestrained, explicit solvent molecular dynamics. This was sufficiently long to observe opening and closing of the structurally important 150-loop and, surprisingly, unbinding and rebinding of oseltamivir. Simulations of oseltamivir complexed to wild-type (WT) H1N1-2009 neuraminidase and five mutants (SN, IR, HY, SNHY, and IRHY) were performed. Each simulation was performed twice, with different starting conditions to ensure statistical independence. To this end, simulations of the complex started from independent setups from two different X-ray crystal structures of the bound form of WT H1N1-2009 neuraminidase. Set 1 (WT1, SN1, IR1, etc.) started from the zanamivir-bound structure [Protein Data Bank (PDB) entry 3TI5],[30] while set 2 (WT2, SN2, IR2, etc.) started from the oseltamivir-bound structure (PDB entry 3TI6).[30] This resulted in 12 independent simulations, totalling 6 μs of dynamics.

MATERIALS AND METHODS

The simulations were set up using the same protocol that we used to study the effect of mutation on H1N1-2009[7] and H7N9 neuraminidase.[39] Initial starting structures were taken from the PDB. Structure 3TI5 (zanamivir complexed with H1N1-2009 neuraminidase[30]) was used to initialize the set 1 simulations, while structure 3TI6 (oseltamivir complexed with H1N1-2009 neuraminidase[30]) was used to initialize set 2. As in our previous validation study,[7] simulations involved just the monomer, which was cut out from the X-ray structure. The coordinates of all crystallographic water molecules were retained, as was the structurally important calcium ion complexed with the protein. Superimposition from 3TI6 was used to generate the initial starting point for oseltamivir in the 3TI5 structure. Hydrogen atoms were added to oseltamivir via a HF/6-31G* optimization using Gaussian 03.[40] This gave the starting point for the WT trajectories. The mutant residues (I222R, S246N, and H274Y) were point mutated from the WT starting structure using the LEaP module of AMBER 12[41] to create the starting points for the IR, HY, SN, IRHY, and SNHY simulations. The mutant residues were built with starting geometries that matched those of the native residues. This was achieved by mirroring the coordinates of shared atoms. All missing hydrogen atoms on the protein were added independently for each system using LEaP[41] using an ionization state of each amino acid residue predicted by PROPKA.[42] The LEaP module of AMBER 12[41] was used to solvate each system independently in a TIP3P[43] water box with approximate dimensions of 90 Å × 90 Å × 90 Å, with chloride counterions added to neutralize the system. The FF03.r1 force field[44] implemented in AMBER 12 was used to model neuraminidase. The atomic charges of oseltamivir were calculated on the basis of the electrostatic potential from a single-point HF/6-31G* calculation using Gaussian 03[40] and fit using the RESP module in AMBER 12.[41] Parameters for oseltamivir were assigned from the generalized AMBER force field (GAFF)[45] using Antechamber[46] and were tested in our previous validation study.[7]

Energy minimization was performed to optimize the position of added hydrogen atoms and water molecules in each system using the pmemd.CUDA module in AMBER 12 (version 12.0, released March 19, 2012).[47] The mixed single-precision/double-precision (SPDP) version of pmemd.CUDA was employed, as we had seen that this produced acceptable results during our preliminary study using AMBER 11.[7] Particle mesh Ewald (PME)[48] was used to account for long-range electrostatics, with a 10 Å real space cutoff, with the same cutoff used for the Lennard-Jones potential. SHAKE[49] was used to constrain bonds involving hydrogen. After minimization, MD simulations were also conducted using pmemd.CUDA.[47] A time step of 2 fs was used, with the simulation divided into thermalization, equilibration, and production phases. In the thermalization step, the temperature was increased linearly to 310 K over a period of 100 ps using canonical (*NVT*) dynamics. A Langevin thermostat was used to maintain temperature, using a collision frequency of 5 ps^{-1}. Next, the system was equilibrated for a further 100 ps of *NVT* dynamics, and then a further 800 ps of isothermal−isobaric (*NPT*) dynamics, with a Langevin thermostat used to maintain a temperature of 310 K, and the isotropic pressure scaling algorithm implemented in pmemd.CUDA used to maintain the pressure at 1 bar, using a pressure relaxation time of 1 ps. Visual inspection of each system confirmed that the starting structures were reasonable and that they closely matched the original 3TI5 or 3TI6 crystal structure. Each system was then equilibrated for a further 20 ns at 310 K and 1 bar, before a further 480 ns of *NPT* dynamics was generated during the production phase. Thermalization, equilibration, and production were conducted using a single M2090 nVidia Tesla GPU per system, with production dynamics of each 67500-atom system running at a rate of approximately 8 ns of sampling per day. The simulations were run in 1 ns blocks, with coordinates of all atoms saved every 10 ps. This generated approximately 22 GB of compressed data per trajectory. In total, running all of the simulations required dedicated access to 12 M2090 GPUs for a period of approximately 60 days and generated ∼300 GB of compressed data.

Interatomic distances were calculated every 200 ps from 20 to 500 ps using Wordom.[50] Distances were calculated between all equivalent donor−acceptor pairs for each salt bridge or hydrogen bond interaction. Figure S1 of the Supporting Information gives the list of atom pairs used for each interaction in each figure. Once all distances had been calculated, a custom script was used to select and plot the shortest distance using the color scales described. The color scale was capped as described in the caption for each figure. For example, a cap between 2 and 8 Å would mean that distances of >8 Å were drawn with the same color as distances of 8 Å, while distances of <2 Å were drawn with the same color as distances of 2 Å.

Root-mean-square deviation (rmsd) calculations were performed using the rmsd module of VMD.[51] The rmsds were calculated every 200 ps from 20 to 500 ps by aligning against the heavy atoms of the protein backbone from the original 3TI6 X-ray structure. When needed, the rmsd of the 150-loop was calculated using the heavy atoms of residues 146−154 (N2 numbering).

The electrostatic surface potentials were calculated using APBS,[52] via the APBS module in VMD.[51] The electrostatic potential was calculated using just the atoms of the protein, with charges assigned using pdb2pqr with the "amber" force field. The protein dielectric was 1.0, and the solvent dielectric was 78.54. The electrostatic potential was plotted on the surface of the protein, as provided via the "QuickSurf" representation, with a radius scale of 0.8. The color scale

ranged from red (−250 mV) through white (0 mV) to blue (250 mV).

Water population maps were calculated using the VOLMAP tool of VMD.[51] The coordinates of the 100 water molecules closest to oseltamivir for snapshots every 200 ps from 20 to 500 ns were extracted using the PTRAJ module of AMBER 12.[41] Each snapshot was aligned using the heavy atoms of the backbone of neuraminidase and the water occupation evaluated using VOLMAP for all water molecules within 8 Å of Q226 on a 0.5 Å grid. A grid point was considered to be occupied if it fell within the van der Waals radius of any water atom for that snapshot. Water occupation was averaged over 480 ns, with isosurfaces at 50 and 80% indicating volumes that were occupied for at least 50% of the 480 ns and 80% of the 480 ns, respectively. When needed, the number of water molecules was approximated using a custom script in VMD.[51] This counted the number of water atoms within 6 Å of the Cδ atom of E277 that were also within 5 Å of any atom of oseltamivir. This number was divided by 3 to give an estimate of the number of water molecules. The calculation used snapshots of the 100 closest water molecules to oseltamivir taken every 200 ps from 20 to 500 ns.

RESULTS AND DISCUSSION

To provide an overview of all of the simulations, the distances between atoms involved in important hydrogen bond or salt bridge interactions between oseltamivir and neuraminidase were calculated every 200 ps between 20 and 500 ns and plotted (Figure 2). The distances chosen were between oseltamivir and key residues highlighted in Figure 1.

Figure 2 shows that, for the most part, complexes of oseltamivir with highly drug resistant mutants (HY, SNHY, and IRHY) of neuraminidase were less stable than those with the WT and less resistant mutants (SN and IR). Hydrogen bond and salt bridge interactions between oseltamivir and neuraminidase broke more readily during the simulations of the drug-resistant mutants, with complete unbinding of oseltamivir observed within 100−300 ns of one of two trajectories for each drug-resistant mutant. In contrast, oseltamivir remained bound in both simulations of the wild-type complex, and both simulations of the less resistant SN mutant complex. In addition, complexes of oseltamivir with the WT and less resistant mutants (IR and SN) showed greater stability, with more interactions that either are maintained or break and then re-form during each 500 ns trajectory. Partial unbinding was observed in only one of these trajectories (IR2) after 450 ns. The relative stability of the oseltamivir−neuraminidase complexes observed in the simulations correlates well with the experimental drug resistance of the mutants. There is a clear difference between the behavior of oseltamivir during the simulations of the WT and less resistant mutants and the simulations of the highly resistant mutants. This, combined with our previous validation study,[7] gives us confidence in the results.

Oseltamivir Unbinding Events. On the time scale of these simulations (500 ns), the unbinding of a drug from a protein is a rare event. It is encouraging that the three trajectories in which oseltamivir unbound were all of the highly drug resistant mutants. While it unwise to generalize observations from these three trajectories to a complete picture of unbinding, analysis of whether and how the mutant residues disrupt the protein−drug complex provides useful insight. To this end, we investigate these three trajectories in more detail.

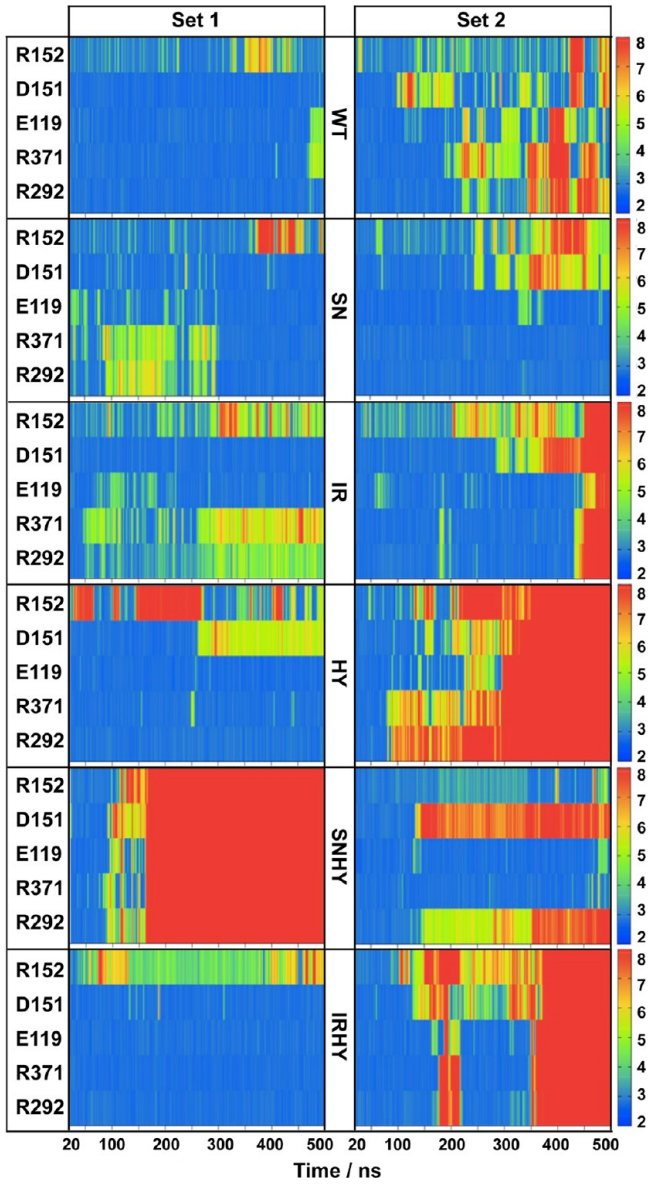

Figure 2. Distances between atoms involved in important interactions between oseltamivir and neuraminidase. These are plotted using a color scale from 2 to 8 Å, with the blue−green color range indicating the presence of salt bridges, hydrogen bonds, or other close contacts and the yellow−red color range indicating broken interactions.

I222R/H274Y. The IRHY2 trajectory is of particular note as it contained two drug unbinding events, separated by a drug rebinding event. Remarkably, in this single 500 ns simulation, oseltamivir unbound from the mutant (at approximately 190 ns), moved into bulk solvent, and then re-bound to neuraminidase (at approximately 250 ns), recovering a binding conformation with an rmsd of 2.4 Å compared to its original binding mode (see Figure S2 of the Supporting Information). Oseltamivir then unbound for a second time (approximately 350 ns), moving again into bulk solvent. MD simulations of unbinding or binding events are extremely rare. This is the first time that oseltamivir unbinding and rebinding have been observed in a single, unbiased, explicit solvent dynamics simulation. Rebinding of the drug recovered a conformation that was very close to the original X-ray structure.

dx.doi.org/10.1021/bi400754t | *Biochemistry* 2013, 52, 8150−8164

In our previous study,[7] we argued that one of the contributors to the drug resistance of the IRHY mutant was the competition between the mutant residue, R222, and 150-loop residue, R152, for a hydrogen bond to the *N*-acetyl group of oseltamivir.[7] The R152 hydrogen bond is one of two interactions that hold the 150-loop in the fully closed conformation while it is bound to oseltamivir. Breaking this hydrogen bond weakens the salt bridge, from D151 to the ammonium group of oseltamivir, allowing the 150-loop to undergo a transition from a closed to an open conformation. Figure 3 shows the competition between the mutant R222 residue and the R152 residue of the 150-loop for the *N*-acetyl oxygen of oseltamivir during the 500 ns of both IRHY simulations. Both trajectories show competition between R222 and R152, with the R152−oseltamivir hydrogen bond broken in both trajectories before approximately 100 ns. The D151 salt bridge is maintained throughout the IRHY1 trajectory, allowing the 150-loop to stay in a closed conformation, and for oseltamivir to remain bound for the full 500 ns. Indeed, after R222 moves away from the *N*-acetyl group, toward interaction with the bulky group of oseltamivir, R152 is able to reapproach the *N*-acetyl group, and the R152 hydrogen bond briefly re-forms. In contrast, in the IRHY2 trajectory, competition from R222 helps break the R152 hydrogen bond at approximately 100 ns. This hydrogen bond partially re-forms at ∼130 ns, but now renewed competition from R222 breaks the R152 hydrogen bond again, with the D151 salt bridge breaking at the same time. This severs the link between the drug and the 150-loop, allowing the loop to open and for oseltamivir to subsequently unbind.

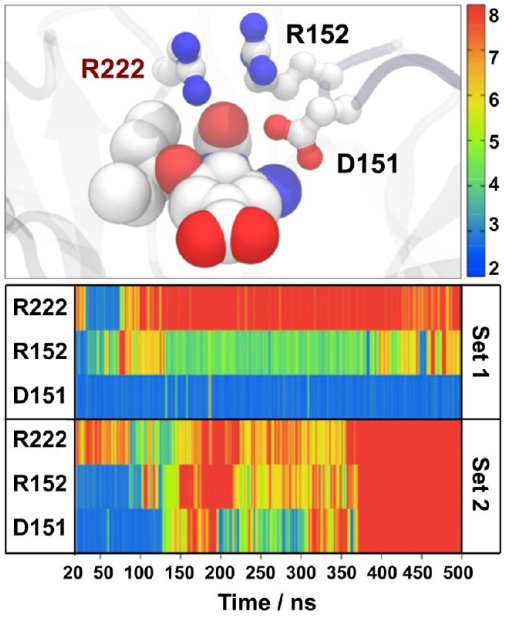

Figure 3. Distances between atoms involved in hydrogen bond and salt bridge interactions between oseltamivir and the D151 and R152 residues in the 150-loop, together with those to the mutant R222 residue. These are plotted using the same color scale as in Figure 2. In the bound complex, oseltamivir is unable to simultaneously hydrogen bond to both R152 and R222. Competition between R152 and R222 leads to breaking of the R152 hydrogen bond, which is accompanied by the breaking of the D151 salt bridge and the opening of the 150-loop in set 2.

IRHY: Unbinding−Rebinding Process. Figure 4 shows snapshots from the IRHY2 trajectory illustrating the unbinding and rebinding processes. It has been suggested that oseltamivir binds poorly to the open conformation of the 150-loop because of poor electrostatic interaction between it and the active site residues.[7] The outside subfigures of Figure 4 show the Poisson−Boltzmann (PB) electrostatic potential calculated at the surface of neuraminidase, viewed from a consistent angle. Regions of positive potential are colored blue, while regions of negative potential are colored red. While there is good electrostatic complementarity between oseltamivir and the binding site for the closed conformation (Figure 4a), opening of the loop leads to a large, negatively charged pocket that encourages oseltamivir to unbind. In addition to changes in electrostatics, visualization of the location of water molecules around oseltamivir reveals interesting behavior. Oseltamivir is initially bound tightly together with a "finger" of six or seven water molecules trapped in a pocket between it and the protein. These water molecules have been highlighted in the inner subfigures of panels a and b of Figure 4. As the 150-loop opened, water molecules from near the binding site could enter through the opening between the loop and oseltamivir (Figure 4c). Bulk water molecules came in contact with the finger of trapped water molecules, with bulk water pushing along this pathway to flood underneath oseltamivir. The increasing number of water molecules underneath the drug pushed against the bulky group of oseltamivir, eventually pushing it out from the bulky group binding pocket (Figure 4d). This appeared to be aided by the mutant R222 residue, which had also moved into a conformation that allowed it to push against the bulky group from below. As the bulky group left the pocket, oseltamivir flipped upside down, making close contact with the residues of the 150-loop. Further opening of the 150-loop occurred in concert with the drug moving up and out of the pocket (Figure 4e), with the drug positioned on top of the loop at the boundary of the active site. From here, oseltamivir was washed out into bulk solvent (Figure 4f).

Rebinding of oseltamivir followed a similar process in reverse. Oseltamivir formed interactions with residues in the 150-loop, with the drug positioned on top of the loop, upside down at the boundary of the active site (Figure 4g,h). This conformation is very similar to that observed during oseltamivir unbinding (Figure 4e). Movement of the 150-loop appeared to manipulate oseltamivir, with the drug spinning around into an approximation of the original binding mode (Figure 4i−k). The 150-loop partially closed over oseltamivir, with the D151 salt bridge re-forming. A large number (≥10) of water molecules were trapped underneath oseltamivir at this point (Figure 4k) compared to the number in the original binding mode (Figure 4a). Some of these excess water molecules diffused out from underneath oseltamivir, pushing past the bulky group, and out via the bulky group binding pocket. After ∼30 ns, many of the excess water molecules had diffused away, and oseltamivir achieved a binding orientation within a 2.4 Å rmsd of its original binding mode. However, this re-bound form persisted for only a further 50 ns, with a second drug unbinding event occurring at ∼300 ns. The second unbinding event was quicker than the first. This may be because the number of water molecules trapped under oseltamivir after rebinding was larger than the number in the original binding mode, and because the interactions between oseltamivir and the 150-loop were not as strong. Figure 2 shows that the hydrogen bond between oseltamivir and R152 did not re-form after rebinding, with the

dx.doi.org/10.1021/bi400754t | *Biochemistry* 2013, 52, 8150−8164

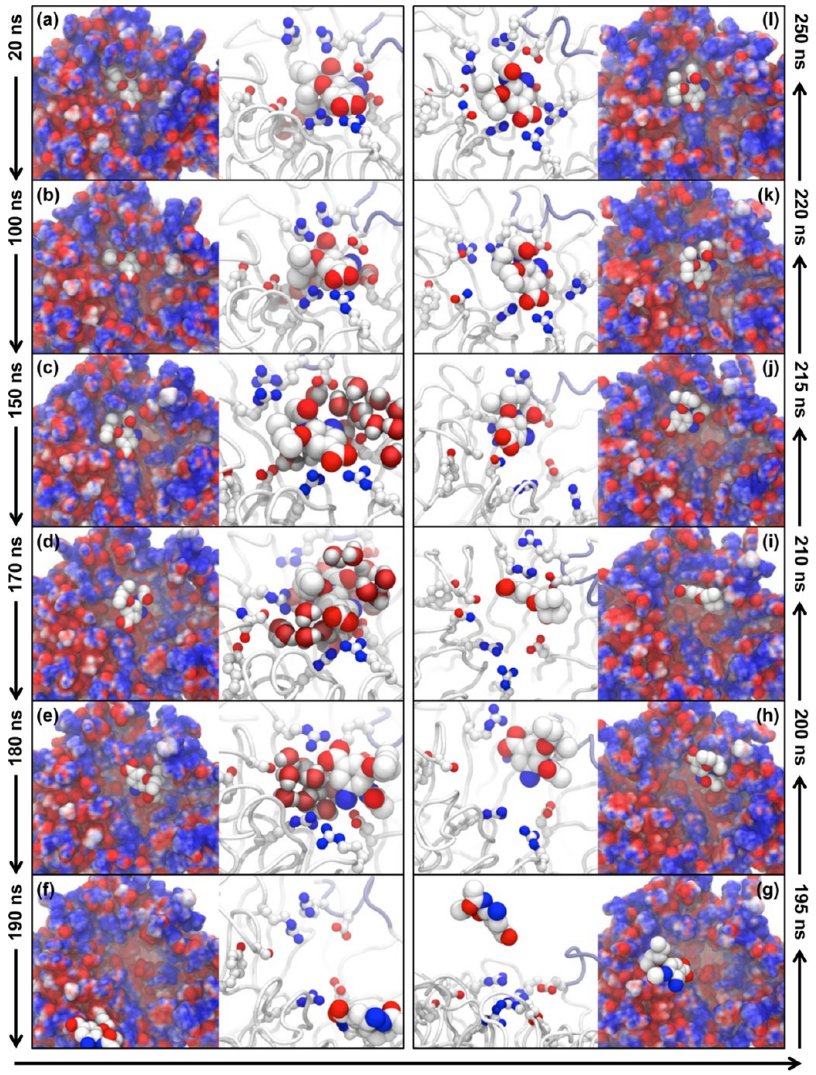

Figure 4. Snapshots illustrating the unbinding and rebinding of oseltamivir observed during the IRHY2 trajectory. The outer subfigures show the electrostatic potential at the surface of the protein, viewed from the same camera position to show the relative position of the drug during the simulation. Regions of negative electrostatic potential are colored red, regions of positive electrostatic potential blue, and neutral regions white. Details of the electrostatic calculation are given in the text. The inner subfigures show close-up views of the drug with important residues indicated. A description of the process highlighted in each snapshot is given in the text.

D151 salt bridge forming only sporadically, and with a longer bond length. On its own, the interaction with D151 could keep the 150-loop partially closed for only ~50 ns, after which time the loop opened and oseltamivir once again unbound. The second unbinding process was very similar to the first, with both the mutant R222 pushing against the bulky group of oseltamivir and water molecules flooding in and solvating the drug once the 150-loop opened.

IRHY and the Behavior of Water. Water molecules are often ignored when visualizing or analyzing biomolecular dynamics trajectories. It is increasingly recognized that water plays an important role in ligand−receptor and protein−drug binding.[53−55] Water played a key role in the IRHY2 simulation, making major contributions to the unbinding and binding pathways. Unbinding of the drug is associated with the release of trapped water molecules. The finger of trapped water molecules highlighted in panels a and b of Figure 4 is present in the 3TI6 X-ray structure and, as seen in Figure 5, was present and stable throughout both WT trajectories. This figure shows the average water occupation between 20 and 500 ns calculated from the two simulations of oseltamivir bound to WT neuraminidase. The six or seven water molecules trapped underneath oseltamivir can be seen to form a clear, stable, fingerlike structure. While this structure was present at the start of the IRHY2 trajectory (Figure 4a,b), opening of the 150-loop allowed bulk water molecules to penetrate behind oseltamivir and flood underneath the drug. This is shown in Figure 6, which plots an approximation of the number of water molecules trapped underneath oseltamivir during both IRHY trajectories. Counting numbers of trapped water molecules is technically challenging, as it is difficult to create a consistent definition of what is meant by "trapped". Instead, we opted to use a count of the number of waters within specified distances of both the drug and the protein. A similar approach was used to count water molecules in another study of neuraminidase.[8] In our case, visualization and manual counting of water molecules showed that this slightly underestimated the number of trapped water molecules but provided a clear signal when the number of trapped waters increased. Figure 6 shows that the number of trapped water molecules remained stable during the

dx.doi.org/10.1021/bi400754t | *Biochemistry* 2013, 52, 8150−8164

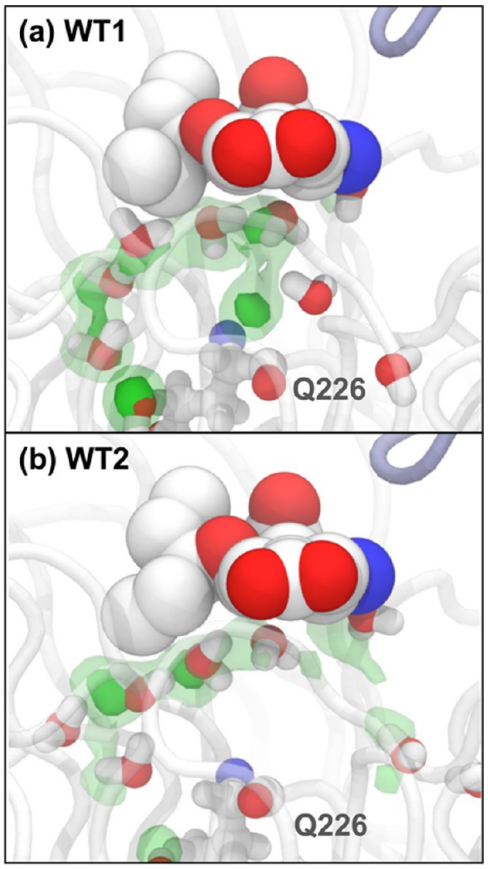

Figure 5. Water occupation beneath oseltamivir from the (a) WT1 and (b) WT2 wild-type simulations. Occupation was calculated for all water molecules within 8 Å of Q226 on a 0.5 Å grid, calculated every 200 ps, and averaged between 20 and 500 ns, using the VOLMAP tool from VMD.[51] Contours are shown for 50% (transparent green) and 80% (solid green) occupation (e.g., a water molecule covered that grid point for more than 50% and more than 80% of the trajectory, respectively). The coordinates of all water molecules within 8 Å of Q226 at 20 ns are shown.

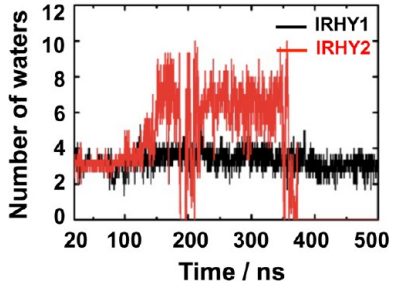

Figure 6. Number of trapped water molecules as calculated every 200 ps from 20 to 500 ns from the IRHY1 and IRHY2 trajectories. The number of trapped water molecules remained stable during the IRHY1 trajectory, in which the 150-loop remained closed. The number of water molecules increases during the IRHY2 trajectory, in concert with the opening of the 150-loop (approximately 130−150 ns).

IRHY1 simulation, during which the 150-loop remained closed. In contrast, the number of trapped water molecules is seen to increase during the IRHY2 trajectory, over the same time scale on which the 150-loop opened (130−150 ns). This increased the density and thus pressure of water underneath oseltamivir, until the bulky group was pushed up and out from the bulky group binding pocket, allowing the trapped water molecules to be freed.

A reverse process occurred during drug rebinding, with water molecules underneath the rebinding oseltamivir being either trapped or displaced. The motion of oseltamivir from the edge of the active site to an approximation of the original binding mode was quite fast (Figure 4h−k), taking at most 20 ns. In contrast, diffusion of excess trapped water molecules from beneath oseltamivir was slower, taking at least 30 ns (Figure 4k,l). This suggests that methods of modeling the kinetics of binding that ignore water molecules or that artificially accelerate water dynamics could miss potentially important effects.

H274Y. In the previous section, the unbinding trajectory representing the IRHY double mutant was analyzed. This was one of three trajectories that contained an unbinding event. The second was the HY2 trajectory. H274 has no direct contact with oseltamivir in the bound complex, yet mutation of H274 to Y causes the strongest resistance to oseltamivir compared to the other single mutants studied here. Similar behavior was seen here, with the 3TI6 HY simulation being the only one of the single-mutant simulations to show complete oseltamivir unbinding. Figure 7 shows key snapshots from this trajectory.

At the beginning of the simulation, the mutant Y274 residue was orientated partially out of the bulky group binding pocket (Figure 7a). It then moved fully into the pocket, moving next to the other residues present there (E276 and S246) (Figure 7b). At this time, the bulky group of oseltamivir began to move up and out from the pocket (Figure 7b). This continued until the salt bridge between oseltamivir and R371 was broken, and the drug moved up, while still interacting with the D151 and R152 residues on the 150-loop (Figure 7c). As the mutant Y274 residue rotated out from the bulky group binding pocket, opening of the 150-loop occurred in concert with oseltamivir moving upward (Figure 7d). The interactions between oseltamivir and D151 and R152 of the 150-loop broke, and the drug detached from the 150-loop, flipping around and dropping upside down into the 150-cavity[11] between the 150-loop and 430-loop (Figure 7e). From here, the 150-loop partially opened and closed twice. During the second closing event, a salt bridge formed between the R152 residue and the carboxylate group of oseltamivir. This salt bridge was maintained as the loop opened, with oseltamivir moving upward and out of the pocket in concert with the motion of the loop (Figure 7f). Further opening of the 150-loop occurred together with the drug moving up and out of the pocket, with the drug positioned upside down on top of the loop at the boundary of the active site (Figure 7g). The interaction between the drug and 150-loop was very similar to that observed during unbinding (Figure 4e) and rebinding (Figure 4h) in the IRHY2 trajectory. Oseltamivir remained associated with the loop, until the flow of water around the edge of the protein broke the drug's interactions and oseltamivir then diffused away into bulk water (Figure 7h).

H274Y and Changes in the Bulky Pocket. The effect of the HY mutation is to reduce the amount of space available in the bulky group binding pocket, making it less able to bind the bulky group and thereby weakening binding of oseltamivir. This is in agreement with previous studies. For example, Wang et al. demonstrated experimentally that mutation of H274 to a larger residue (e.g., tyrosine or phenylalanine) resulted in a significant loss of oseltamivir binding efficacy.[31] While there is agreement that the HY mutation confers resistance because of the

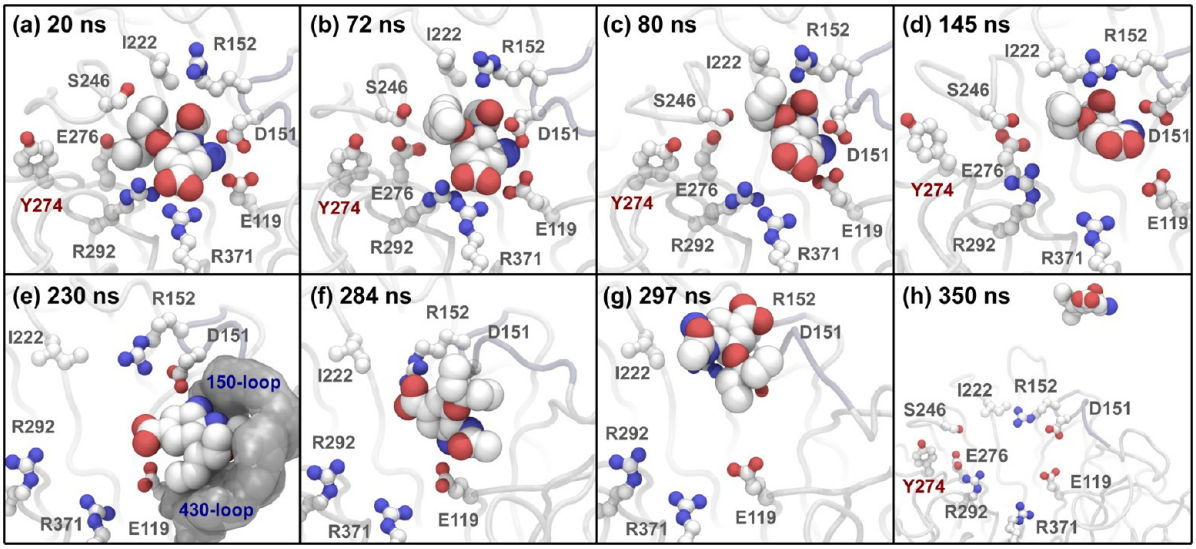

Figure 7. Snapshots illustrating the unbinding of oseltamivir observed during the HY2 trajectory. A description of the process highlighted in each snapshot is given in the text.

reduction in the size of the pocket, exactly how this occurs is open to debate. There are three main hypotheses.

(1) Analysis of X-ray crystal structures suggested that crowding disrupts or prevents the formation of a key salt bridge between E276 and R224 (see Figure S3 of the Supporting Information).[31,32] This prevents the bulky group pocket from forming fully, thus disrupting binding of the drug. This was supported by subsequent computational studies that suggested that the lower free energy for binding of oseltamivir to the HY mutant could be a result of the loss of the salt bridge between E276 and R224.[35,37]

(2) Comparison of molecular dynamics trajectories of oseltamivir bound to the WT and HY variants of H5N1 neuraminidase showed that Y274 did not restrict the reorientation of E276 needed to form the salt bridge and create a stable bulky group binding pocket.[8,10,36,38] Instead, the simulations and X-ray structure of H274Y complexed with oseltamivir in N1 suggested that the exact position of E276 was changed, causing a reduction in the size of the pocket.[10,33,34] This, coupled with the presence of the polar hydroxy group of Y274, disrupted the hydrogen bond framework in the pocket, reducing the binding efficacy of oseltamivir. Disruption of hydrogen bonding in the cavity has also been suggested by Hamiltonian replica exchange[36] and steered MD studies.[38]

(3) Simulations of oseltamivir complexed to the HY mutant showed infiltration of water molecules into the bulky group binding pocket.[8,9] This suggested that the HY mutant somehow encouraged penetration by water, disrupting the bulky group, and thereby reducing the binding affinity of oseltamivir.

Analysis of the HY2 trajectory shows support for the last two hypotheses and disagrees with the first. Y274 did not restrict the reorientation of E276, which was seen to be free to form a strong salt bridge with R224 (Figure S3 of the Supporting Information). At the start of unbinding, Y274 pushed against the carboxylate group of E276, pushing it against the bulky group of oseltamivir (Figure 7b). In addition, visualization of water molecules in the binding site showed that this push was supported by an increased degree of penetration of water molecules into the bulky group binding pocket. Figure 8 shows an estimate of the number of water molecules trapped underneath oseltamivir during the two simulations of the HY

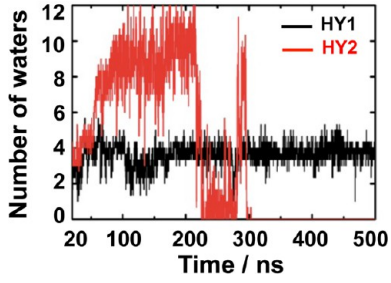

Figure 8. Number of trapped water molecules as calculated every 200 ps from 20 to 500 ns from the HY1 and HY2 trajectories. The number of trapped water molecules remained stable during the HY1 trajectory, in which the Y274 residue pointed out of the bulky group binding pocket. The number of water molecules increased during the HY2 trajectory, in which the Y274 residue pointed into the pocket. Flooding occurred in concert with penetration of water into the bulky group binding pocket (50−80 ns).

mutant. This was calculated using the same procedure as in Figure 6, and as before, while it underestimates the number of trapped water molecules, it is a good indicator of flooding. This shows that the number of water molecules trapped underneath oseltamivir during the HY2 trajectory increased significantly before drug unbinding. This was in contrast to the HY1 trajectory, during which the number of trapped water molecules remained stable, and oseltamivir remained bound. Figure 9 shows the behavior of water molecules during the unbinding process in the HY2 trajectory. As noted when discussing the unbinding of neuraminidase from the IRHY mutant, binding of oseltamivir traps a finger of water molecules between the protein and the drug. This finger of water is present and stable during the first 50 ns of the HY2 trajectory (Figure 9a,b). During the HY1 trajectory, the mutant Y274 residue pointed away from the bulky group binding pocket. In contrast, at the start of the HY2 trajectory, Y274 pointed into the pocket. In this conformation, the hydroxyl group of Y274 stabilized an additional water molecule near it and E276. This water molecule acted as an anchor from which a bridge of water molecules formed. This bridge was stable and provided a conduit by which more water molecules could penetrate into

dx.doi.org/10.1021/bi400754t | *Biochemistry* 2013, 52, 8150−8164

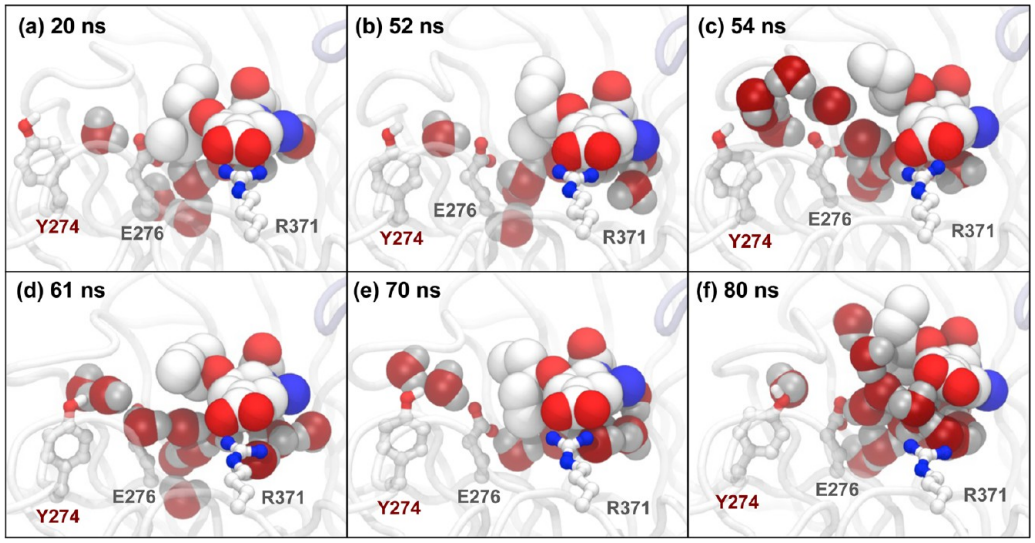

Figure 9. Snapshots illustrating the penetration of water molecules in the bulky group binding pocket from the HY2 trajectory. The Y274 residue pointed into the bulky group binding pocket stabilizing a water molecule between it and E276. This provided an anchor from which a bridge of water molecules could grow. Water molecules then move past the bulky group of oseltamivir, flooding underneath the drug, until it is lifted up, breaking the salt bridge to R371.

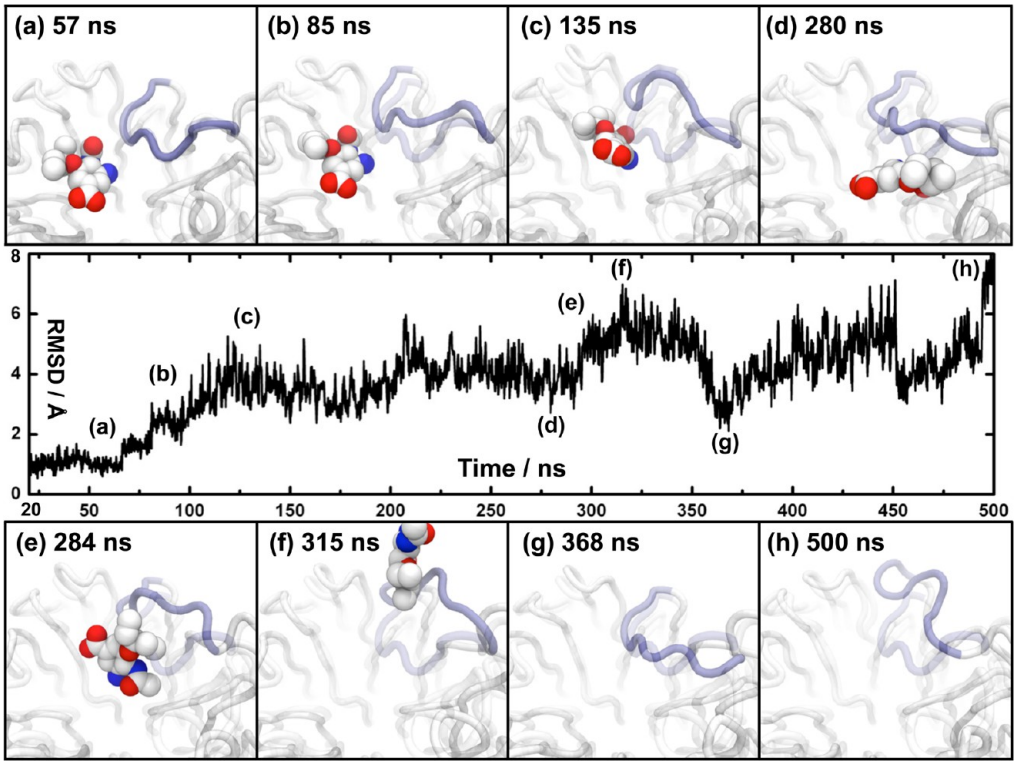

Figure 10. Snapshots illustrating the motion of the 150-loop (blue) during unbinding of oseltamivir observed in the HY2 trajectory. The rmsd of the backbone atoms of the 150-loop is calculated versus its conformation in the 3TI6 crystal structure (translucent in the snapshots). The rmsd was calculated using the rmsd module of VMD[51] and evaluated every 200 ps between 20 and 500 ns. A description of the process highlighted in each snapshot is given in the text.

the bulky group binding pocket (Figure 9c). This bridge, supported by hydrogen bonding with Y274, provided a connection to the finger of water molecules trapped underneath oseltamivir (Figure 9c,d). This connection allowed water molecules to flow underneath oseltamivir, both simultaneously pushing the bulky group out from the bulky group binding pocket and increasing the number of water molecules trapped underneath the drug. Occasionally, the bridge of water molecules was broken, as the bulky group of oseltamivir rebound to the pocket (Figure 9e). However, the number of water molecules, and hence pressure from water, trapped underneath oseltamivir had increased, helping to lift the drug up, breaking the key salt bridge between oseltamivir and R371 (Figure 9f).

H274Y and Behavior of the 150-Loop. As in the IRHY2 trajectory, the 150-loop played a key role during the unbinding

dx.doi.org/10.1021/bi400754t | *Biochemistry* 2013, 52, 8150−8164

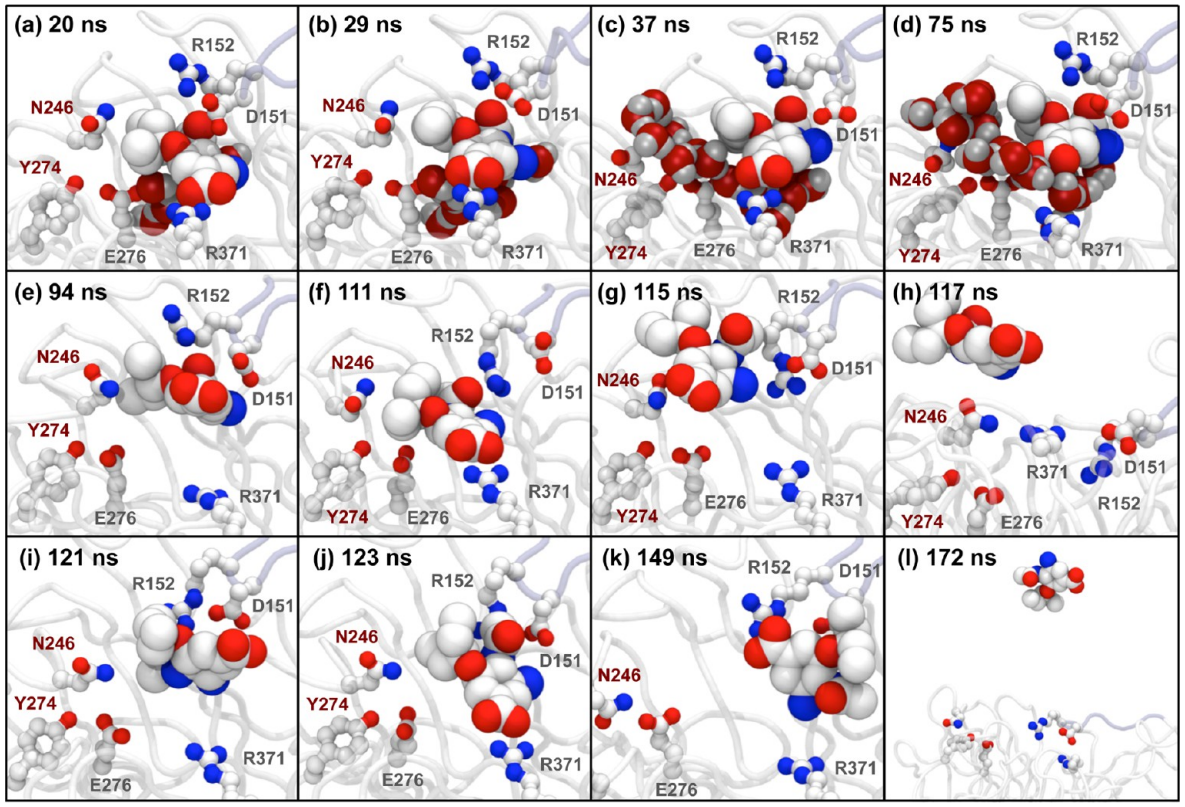

Figure 11. Snapshots illustrating the unbinding of oseltamivir observed during the SNHY1 trajectory. Important residues involved in the unbinding mechanism are highlighted, together with water molecules that are trapped underneath oseltamivir when it is bound to the protein, and water molecules that move to penetrate the bulky group binding pocket.

process in HY2. The motion of the 150-loop appeared to correlate with important stages of the unbinding mechanism. Figure 10 shows the 3TI6 crystal structure of neuraminidase (transparent) versus key snapshots taken at different points along the MD trajectory. The rmsd of the 150-loop versus the crystal structure conformation is calculated every 200 ps between 20 and 500 ns from the HY2 trajectory. Higher values indicate a more open form of the loop, and lower values indicate a more closed form. Figure 10a shows the system at 57 ns. This is near the start of the trajectory, when the conformation of the protein closely matched the crystal structure, and the loop was closed. As described above, between 50 and 80 ns the unbinding event was initiated when the bulky group of oseltamivir moved up and out of the bulky group binding pocket. This can be seen in Figure 10b. The bulky group of the drug is pushed upward, and the drug now sits at a slight angle in the binding site. As is seen in the rmsd plot, this occurs over the same time period as the 150-loop began to slightly open. Further opening of the loop between 85 and 135 ns occurred as the drug moved up and away from the binding site (Figure 10c). The drug then detached from the 150-loop and fell into the 150-cavity. The rmsd plot shows how the 150-loop partially closed (175 ns), opened (210 ns), and closed (280 ns). It was during this second closing event that it came into contact with oseltamivir (Figure 10d), forming a salt bridge to the drug. The rmsd plot shows the 150-loop fully opening between 280 and 315 ns, at the same time as the drug moves up and out from the binding site (Figure 10e,f) and onto the surface of the protein. From here, the drug detached and diffused into bulk water. The 150-loop closed [370 ns (Figure 10g)], opened (450 ns), closed (460 ns), and opened [500 ns (Figure 10h)], while free of the drug.

Crystallographic studies show that the 150-loop exists in both open and closed forms.[11,12] Simulation studies show motion of the loop between the two states.[7,56−58] MD studies of neuraminidase from H5N1 showed that the 150-loop opened more and was more flexible than in the observed X-ray structure.[56−58] Our observations from the IRHY2 and HY2 trajectories suggest that as well as being highly flexible, the dynamics of the 150-loop could have a biological function. The random opening and closing of the 150-loop appeared to be coupled with the random motion of the drug; e.g., loop opening events occur at the same time as the drug moves up and out of the binding pocket. As oseltamivir is based on a transition state analogue for neuraminidase, our simulations suggest that motion of the loop may play a role in the mechanism of the enzyme; i.e., closing of the loop aids binding of the substrate, while opening of the loop aids in the release of the product. More study is needed to investigate this theory, as an equally valid conclusion from this simulation is that motion of the loop could have hindered release of oseltamivir, so the loop may equally hinder release of the product.

S246N/H274Y. The third and final trajectory to contain a complete unbinding event was SNHY1. S246 forms part of the bulky group binding pocket. Despite this, a single mutation to the larger N246 residue confers upon neuraminidase only mild resistance to oseltamivir (see Table 1).[26] However, the recent emergence of a dual SNHY mutant, which is at least 5 times more resistant than the already drug-resistant HY mutant, is a serious concern. Like that of the IRHY double mutant, the binding affinity of oseltamivir for the SNHY double mutant is

dx.doi.org/10.1021/bi400754t | *Biochemistry* 2013, 52, 8150−8164

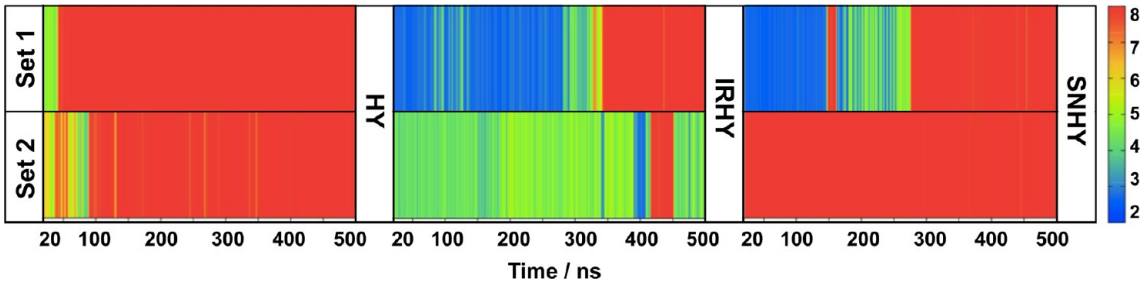

Figure 12. Distances between Y274 and E276 calculated every 200 ps from 20 to 500 ns from all simulations involving the H274Y mutation. The color scale ranges from 2 to 8 Å, with blue−green values indicating that the Y274 residue is pointing inward, toward the bulky group binding pocket, and red values indicating that Y274 is pointing away from the pocket.

reduced to such an extent that it would not be an effective antiviral treatment for this strain of influenza.[26]

In agreement with the observed drug resistance, Figure 2 shows that the neuraminidase−oseltamivir complexes in the two SN simulations were very stable, while the complexes in the SNHY trajectories were more unstable, with drug unbinding occurring in the early part of the SNHY1 trajectory. The SNHY1 trajectory contains partial unbinding, partial rebinding, and full unbinding events. Figure 11 shows key snapshots from the unbinding process observed during this trajectory. The unbinding event appeared to start right at the beginning of the trajectory (Figure 11a). The mutant Y274 residue was pointing into the bulky group binding pocket, located against the mutant N246, which itself was positioned against the bulky group of oseltamivir. The combination of the increased size of Y274 and the increased size of N246 significantly reduced the space available for binding the bulky group. This is in agreement with structural studies.[26] The drug appeared to be pushed away at an angle (Figure 11b). The loop containing N246 moved down, opening a channel into which water molecules could penetrate the bulky group binding pocket (Figure 11c). These water molecules formed a bridge that was stabilized by hydrogen bonding to both of the mutant residues (S246 and Y274) and to E276 (also Figure 11c). The bridge of water molecules was connected with the finger of water molecules trapped below oseltamivir, allowing additional water molecules to flood underneath the drug (see Figure S4 of the Supporting Information). As was observed in the HY2 trajectory, flooding of water underneath oseltamivir, together with interactions with residues on the partially opening 150-loop, helped to break the key salt bridge between the drug and R371 (Figure 11d). From here, partial opening of the 150-loop occurred together with upward motion of oseltamivir (Figure 11e), until the drug detached from the loop and re-bound to the R371 residue (Figure 11f). This salt bridge was the only direct attachment between oseltamivir and neuraminidase, and it quickly broke (Figure 11g), allowing the drug to drift out of the binding pocket (Figure 11h). The drug diffused across the binding pocket, hydrogen bonding and attaching to the residues of the 150-loop (Figure 11i). The motion of the 150-loop helped return the drug to the binding pocket, as oseltamivir once again formed the key salt bridge to R371 (Figure 11j). This salt bridge was the only direct attachment to the protein, and as before, this salt bridge broke. Breaking and re-forming of the salt bridge appeared to be influenced by the position of the 150-loop. The R152 residue competed with R371 for the salt bridge, occasionally breaking the salt bridge and flipping oseltamivir upside down, attaching it to the 150-loop (Figure 11k), in a conformation similar to that observed in the IRHY2 and HY2 trajectories. Unlike the IRHY2 and HY2 unbinding events, the 150-loop remained closed. The salt bridge to R152 broke, and the drug diffused up and away from the binding site without any cooperative motion by the 150-loop (Figure 11l).

Oseltamivir-Bound Trajectories. Analysis of the detail of the unbinding events has provided a unique insight into the molecular basis of oseltamivir resistance. For the computational model and software employed, oseltamivir unbinding was driven by a combination of competition between the mutant R222 residue and the 150-loop (for IRHY2), increased steric crowding in the bulky group binding pocket (for HY2 and SNHY1), and penetration of water molecules underneath oseltamivir via a channel between the drug and the 150-loop (IRHY2) or by pushing open a conduit through the bulky group binding pocket (HY2 and SNHY1). An obvious question is why these same drivers were not present or were present and did not lead to unbinding in the simulations in which oseltamivir remained bound. A general explanation is that the conformational changes and processes observed in the three unbinding trajectories were relatively rare events and would not be expected to occur during every 500 ns simulation of neuraminidase. More detailed explanations can be found by comparing the three unbinding trajectories with the nine in which the drug remained bound.

Effect of Y274. The reduced size of the bulky group binding pocket caused by the increased size of the Y274 mutant residue was a key contributer to unbinding observed during the HY and SNHY trajectories. Y274 was seen to be highly mobile, moving between configurations where it was pointing either into or out from the bulky group binding pocket. Figure 12 shows the distance between Y274 and E276 for all of the trajectories that included the Y274 mutant. This distance was chosen as it was a good indicator of the configuration of Y274, with short distances (blue−green values in the figure) indicating that the residue was pointing into the pocket and larger distances (yellow−red values) indicating it was pointing out of the pocket. For most of the trajectories, Y274 pointed out from the pocket. However, it was always pointing into the pocket whenever the drug unbinding events in IRHY2, HY2, and SNHY1 were initiated, and for the majority of each of the entire unbinding processes (50−80 ns for HY2, 100−170 ns for IRHY2, and 20−75 ns for SNHY1). This observation suggests that drug unbinding was not observed during the HY1 and SNHY2 trajectories because, by chance, Y274 was pointing out of the pocket. This also suggests a possible explanation for why unbinding was observed on shorter time scales than perhaps would be expected on the basis of the binding free energy of oseltamivir for this model.[a] All of the HY mutant trajectories started from conformations with Y274 pointing into the pocket,

dx.doi.org/10.1021/bi400754t | *Biochemistry* 2013, 52, 8150−8164

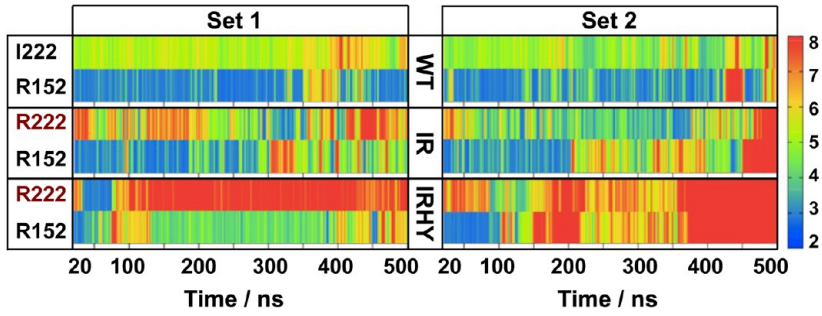

Figure 13. Distances between atoms involved in hydrogen bond interactions between the *N*-acetyl group of oseltamivir and the R152 and mutant R222 residues in the IR and IRHY trajectories. This is compared with corresponding distances for the WT trajectories. These are plotted using the same color scale as in Figure 2, with blue−green values indicating the presence of a hydrogen bond. In the bound complex, oseltamivir is unable to simultaneously hydrogen bond to both R152 and R222. Competition from R222 leads to breaking of the R152 hydrogen bond to oseltamivir.

which would artificially overcome any barrier between the "pointing out" and "pointing in" conformations. This would accelerate unbinding compared to trajectories that started from a pointing out conformation. This suggests that further investigation into the orientational preference and thermodynamics of Y274 is necessary, with our simulations suggesting that the pointing out conformation is more stable.

Effect of N246. N246 contributed to the unbinding of oseltamivir in the SNHY1 trajectory both via its increased size compared to that of S246 and via its support of water penetration via the bulky group binding pocket. N246 supports water penetration, with this observed in the SN1 trajectory and both SNHY trajectories (Figure 11 and Figures S4 and S5 of the Supporting Information). However, the effect of N246 alone was not sufficient to trigger unbinding. Unbinding was observed only in the SNHY1 trajectory, when Y274 pointed into the bulky group pocket and supported both the reduction in space available to bind oseltamivir and the increased extent of water penetration. This suggests that the SNHY double mutant is more oseltamivir resistant than the single HY mutant as N246 supports Y274 in reducing the size of the bulky group binding pocket and in supporting the penetration of water. It is interesting to note that water penetration was a reversible process in the SN1 trajectory. This trajectory lacked the Y274 mutant, thereby allowing a stable binding mode to be retained where N246 supported both the passage of water molecules into and out from underneath oseltamivir (see Figures S4−S6 of the Supporting Information).

Effect of R222. To understand the role of the IR mutation, it is useful to examine the amount of competition observed between the mutant R222 residue and the R152 residue for hydrogen bonding to oseltamivir. This is shown in Figure 13 for the IR and IRHY trajectories, together with an equivalent distance calculated between I222 and oseltamivir for the WT trajectories. This shows that the hydrogen bond between oseltamivir and R152 is not particularly strong, even during the WT trajectories. It breaks and re-forms a large number of times in each trajectory, with the presence of R222 appearing to encourage breaking of the hydrogen bond and discourage re-forming. The interactions with D151 and R152 must both be broken to allow the 150-loop to fully open, and for the conduit that allows penetration of water molecules to form. The salt bridge between oseltamivir and D151 is much stronger than the hydrogen bond to R152, with Figure 2 showing that this interaction breaks less frequently. This salt bridge appeared to be stronger in the set 1 simulations compared to those of set 2. This is despite only a small difference in rmsd (0.2 Å) of the heavy atoms of neuraminidase between the original 3TI5 and 3TI6 crystallographic structures. This means that the probability of both the D151 and R152 interactions being broken in the set 2 simulations was greater than during the set 1 simulations. For example, both interactions were occasionally and temporarily broken together during the WT2 wild-type trajectory. This was accompanied by only slight destabilization of the binding mode of oseltamivir, together with associated penetration of water into the binding pocket (see Figures S4 and S6 of the Supporting Information). In contrast, breaking of both the D151 and R152 interactions occurred more frequently during the IR2 and IRHY2 trajectories, with competition from R222 allowing these breaks to persist. This gave sufficient time for the 150-loop to fully open and for water molecules to fully penetrate the pocket underneath oseltamivir (Figure S6 of the Supporting Information). This occurred early during the IRHY2 trajectory, giving sufficient time to observe complete drug unbinding, rebinding, and unbinding. In contrast, it occurred only after ∼350 ns during the IR trajectory. The loop fully opened at ∼400 ns, after which time the drug partially unbound (450 ns) and then re-bound rotated 180° in the binding site [500 ns (see Figure S6 of the Supporting Information)]. This suggests that while competition from R222 was present in all of the IR and IRHY trajectories, it was only because the D151 interaction appeared to be weaker in the set 2 trajectories that the rare event of both the D151 and R152 interactions being broken, and thus 150-loop opening, could be observed during the 500 ns time span of the simulations.

■ CONCLUSION

Multiple oseltamivir unbinding and rebinding events were observed during several of the simulations of the drug-resistant mutants. Complete unbinding occurred in the IRHY2, HY2, and SNHY1 trajectories. Near-complete rebinding was seen in the IRHY2 trajectory, with partial rebinding witnessed in the SNHY1 trajectory. To the best of our knowledge, this is the first observation of oseltamivir unbinding and rebinding to neuraminidase observed during individual, unbiased, explicit solvent MD trajectories. Molecular-level rationalizations of oseltamivir resistance were revealed by analysis of these unbinding trajectories. For the computational model and software employed, oseltamivir unbinding was driven by a combination of competition between the mutant R222 residue and the R151 residue on the 150-loop (IR mutation), the reduction in the size of the bulky group binding pocket (HY mutation), and the penetration of water molecules underneath oseltamivir via a channel between the drug and the opening

dx.doi.org/10.1021/bi400754t | *Biochemistry* 2013, 52, 8150−8164

150-loop (IR) or by pushing open a conduit through the bulky group binding pocket (HY and SN). These observations were supported by analysis of the trajectories during which unbinding was not observed. In addition, analysis revealed the important role played by water molecules that are isolated in pockets upon drug binding. One of the drivers for the unbinding of oseltamivir was the opening of conduits that allowed flooding of the isolated pocket of water molecules trapped underneath the drug. The increasing density of water below oseltamivir supported pushing the drug up and out of the pocket, thereby releasing all of the trapped water molcules. Drug rebinding was observed to be a slow process, with a significant proportion of the time required to allow excess trapped water molecules to diffuse out from the pocket below oseltamivir. This indicates that the dynamics of water molecules in binding sites is very important in understanding drug binding and kinetics. Finally, we observed that the dynamics of the 150-loop was closely related to the motion of the drug during unbinding and rebinding; e.g., opening of the loop occurred together with movement of the drug up and out of the binding site. This dynamic behavior emerged naturally out of the random thermal motion of the atoms and residues in the loop. The similarity of oseltamivir to a transition state analogue for neuraminidase suggests that the dynamics of the loop may play a functional role in the enzyme, with loop closing aiding in binding of the substrate and loop opening aiding in the release of the product. More study is needed to investigate this hypothesis, to provide firm evidence to demonstrate whether loop motion actively helped or hindered substrate binding and product release.

■ ASSOCIATED CONTENT

Supporting Information

The list of atom pairs used for all of the distance calculations (Figure S1), rmsds of oseltamivir and neuraminidase during the IRHY2 trajectory (Figure S2), distances of key atoms showing the presence of the E276−R224 salt bridge in the WT, HY, IRHY, and SNHY trajectories (Figure S3), approximation of the number of trapped water molecules calculated for all trajectories (Figure S4), snapshots from the SN1 and SNHY2 trajectories showing N246 supporting penetration of water molecules via the bulky group binding pocket (Figure S5), and the final configuration of oseltamivir and neuraminidase at 500 ns for all of the trajectories (Figure S6). This material is available free of charge via the Internet at http://pubs.acs.org.

■ AUTHOR INFORMATION

Corresponding Authors

*E-mail: adrian.mulholland@bristol.ac.uk. Phone: +44-(0)117-928-9097. Fax: +44-(0)117-9277985.

*E-mail: christopher.woods@bristol.ac.uk.

Funding

We thank the EPSRC (EP/I030395/1) for funding this work. A.J.M. is an EPSRC leadership fellow.

Notes

The authors declare no competing financial interest.

■ ACKNOWLEDGMENTS

This was conducted with the kind support and computational facilities of eInfraStructureSouth (http://einfrastructuresouth.ac.uk) and the University of Bristol Advanced Computing Research Center (http://www.bris.ac.uk/acrc). Data storage was provided by the University of Bristol Research Data Storage Facility (RDSF). We particularly thank D. Ross for his support installing and configuring AMBER 12 on the Emerald GPU cluster and C. Gardiner and B. Cregan for their support arranging and administering our storage space on the RDSF.

■ ADDITIONAL NOTE

[a]Exploratory absolute binding free energy calculations using the WaterSwap[59] binding method show strong binding between the model of oseltamivir and neuraminidase, with free energies calculated in a range of −20 to −30 kcal/mol for the equilibrated complex of oseltamivir bound to both the WT and IRHY double mutant. WaterSwap calculates absolute binding free energies using thermodynamic integration along a dual-topology reaction coordinate that exchanges a ligand with an equivalent volume of water in the protein active site. These calculations are ongoing and will be described in a future manuscript.

■ REFERENCES

(1) Kawai, N., Ikematsu, H., Kawashima, T., Maeda, T., Ukai, H., Hirotsu, N., Iwaki, N., and Kashiwagi, S. (2013) Increased symptom severity but unchanged neuraminidase inhibitor effectiveness for A(H1N1)pdm09 in the 2010−2011 season: Comparison with the previous season and with seasonal A(H3N2) and B. *Influenza Other Respir. Viruses 7*, 448−455.

(2) Gasink, L. B., Linkin, D. R., Fishman, N. O., Bilker, W. B., Weiner, M. G., and Lautenbach, E. (2009) Stockpiling drugs for an avian influenza outbreak: Examining the surge in oseltamivir prescriptions during heightened media coverage of the potential for a worldwide pandemic. *Infection Control and Hospital Epidemiology 30*, 370−376.

(3) Hansen, E., Day, T., Arino, J., Wu, J., and Moghadas, S. M. (2010) Strategies for the use of oseltamivir and zanamivir during pandemic outbreaks. *Canadian Journal of Infectious Diseases and Medical Microbiology 21*, e28−e63.

(4) Wan Po, A. L., Farndon, P., and Palmer, N. (2009) Maximizing the value of drug stockpiles for pandemic influenza. *Emerging Infect. Dis. 15*, 1686−1687.

(5) Whitley, R. J., Boucher, C. A. B., Lina, B., Nguyen-Van-Tam, J. S., Osterhaus, A., Schutten, M., and Monto, A. S. (2013) Global assessment of resistance to neuraminidase inhibitors: 2008−2011. The influenza resistance information study (IRIS). *Clin. Infect. Dis. 56*, 1197−1205.

(6) Thorlund, K., Awad, T., Boivin, G., and Thabane, L. (2011) Systematic review of influenza resistance to the neuraminidase inhibitors. *BMC Infect. Dis. 11*, 134.

(7) Woods, C. J., Malaisree, M., Pattarapongdilok, N., Sompornpisut, P., Hannongbua, S., and Mulholland, A. J. (2012) Long time scale GPU dynamics reveal the mechanism of drug resistance of the dual mutant I223R/H275Y neuraminidase from H1N1-2009 influenza virus. *Biochemistry 51*, 4364−4375.

(8) Park, J. W., and Jo, W. H. (2009) Infiltration of water molecules into the oseltamivir-binding site of H274Y neuraminidase mutant causes resistance to oseltamivir. *J. Chem. Inf. Model. 49*, 2735−2741.

(9) Vergara-Jaque, A., Poblete, H., Lee, E. H., Schulten, K., González-Nilo, F., and Chipot, C. (2012) Molecular basis of drug resistance in A/H1N1 virus. *J. Chem. Inf. Model. 52*, 2650−2656.

(10) Malaisree, M., Rungrotmongkol, T., Nunthaboot, N., Aruksakunwong, O., Intharathep, P., Decha, P., Sompornpisut, P., and Hannongbua, S. (2009) Source of oseltamivir resistance in avian influenza H5N1 virus with the H274Y mutation. *Amino Acids 37*, 725−732.

(11) Russell, R. J., Haire, L. F., Stevens, D. J., Collins, P. J., Lin, Y. P., Blackburn, G. M., Hay, A. J., Gamblin, S. J., and Skehel, J. J. (2006) The structure of H5N1 avian influenza neuraminidase suggests new opportunities for drug design. *Nature 443*, 45−49.

(12) Li, Q., et al. (2010) The 2009 pandemic H1N1 neuraminidase N1 lacks the 150-cavity in its active site. *Nat. Struct. Mol. Biol. 17*, 1266−1268.
(13) Varghese, J. N., McKimm-Breschkin, J. L., Caldwell, J. B., Kortt, A. A., and Colman, P. M. (1992) The structure of the complex between influenza virus neuraminidase and sialic acid, the viral receptor. *Proteins 14*, 327−332.
(14) Zhu, X., McBride, R., Nycholat, C. M., Yu, W., Paulson, J. C., and Wilson, I. A. (2012) Influenza virus neuraminidases with reduced enzymatic activity that avidly bind sialic acid receptors. *J. Virol. 86*, 13371−13383.
(15) De Clercq, E. (2006) Antiviral agents active against influenza A viruses. *Nat. Rev. Drug Discovery 5*, 1015−1025.
(16) Kim, C. U., Lew, W., Williams, M. A., Liu, H., Zhang, L., Swaminathan, S., Bischofberger, N., Chen, M. S., Mendel, D. B., Tai, C. Y., Laver, W. G., and Stevens, R. C. (1997) Influenza neuraminidase inhibitors possessing a novel hydrophobic interaction in the enzyme active site: Design, synthesis and structural analysis of carbocyclic sialic acid analogues with potent anti-influenza activity. *J. Am. Chem. Soc. 119*, 681−690.
(17) *Orange Book: Approved Drug Products with Therapeutic Equivalence Evaluations* (1999) U.S. Food and Drug Administration, Washington, DC.
(18) Le, Q. M., et al. (2005) Avian flu: Isolation of drug-resistant H5N1 virus. *Nature 437*, 1108.
(19) Hurt, A. C., Holien, J. K., Parker, M. W., and Barr, I. G. (2009) Oseltamivir resistance and the H274Y neuraminidase mutation in seasonal, pandemic and highly pathogenic influenza viruses. *Drugs 69*, 2523−2531.
(20) McKimm-Breschkin, J. L. (2013) Influenza neuraminidase inhibitors: Antiviral action and mechanisms of resistance. *Influenza Other Respir. Viruses 1*, 25−36.
(21) Gubareva, L. V., Trujillo, A. A., Okomo-Adhiambo, M., Mishin, V. P., Deyde, V. M., Sleeman, K., Nguyen, H. T., Sheu, T. G., Garten, R. J., Shaw, M. W., Fry, A. M., and Klimov, A. I. (2010) Comprehensive assessment of 2009 pandemic influenza A (H1N1) virus drug susceptibility in vitro. *Antiviral Ther. 15*, 1151−1159.
(22) Nguyen, H. T., Trujillo, A. A., Sheu, T. G., Levine, M., Mishin, V. P., Shaw, M., Ades, E. W., Klimov, A. I., Fry, A. M., and Gubareva, L. V. (2012) Analysis of influenza viruses from patients clinically suspected of infection with an oseltamivir resistant virus during the 2009 pandemic in the United States. *Antiviral Res. 93*, 381−386.
(23) Nguyen, H. T., Fry, A. M., Loveless, P. A., Klimov, A. I., and Gubareva, L. V. (2010) Recovery of a multidrug-resistant strain of pandemic influenza A 2009 (H1N1) virus carrying a dual H275Y/I223R mutation from a child after prolonged treatment with oseltamivir. *Clin. Infect. Dis. 51*, 983−984.
(24) van der Vries, E., Stelma, F. F., and Boucher, C. A. (2010) Emergence of a multidrug-resistant pandemic influenza A (H1N1) virus. *N. Engl. J. Med. 363*, 1381−1382.
(25) Pizzorno, A., Abed, Y., Bouhy, X., Beaulieu, E., Mallett, C., Russell, R., and Boivin, G. (2012) Impact of mutations at residue I223 of the neuraminidase protein on the resistance profile, replication level, and virulence of the 2009 pandemic influenza virus. *Antimicrob. Agents Chemother. 56*, 1208−1214.
(26) Hurt, A. C., Lee, R. T., Leang, S. K., Cui, L., Deng, Y. M., Phuah, S. P., Caldwell, N., Freeman, K., Komadina, N., Smith, D., Speers, D., Kelso, A., Lin, R. T., Maurer-Stroh, S., and Barr, I. G. (2011) Increased detection in Australia and Singapore of a novel influenza A(H1N1)-2009 variant with reduced oseltamivir and zanamivir sensitivity due to a S247N neuraminidase mutation. *Euro Surveillance 16*, 19884.
(27) Eshaghi, A., Patel, S. N., Sarabia, A., Higgins, R. R., Savchenko, A., Stojios, P. J., Li, Y., Bastien, N., Alexander, D. C., Low, D. E., and Gubbay, J. B. (2011) Multidrug-resistant pandemic (H1N1) 2009 infection in immunocompetent child. *Emerging Infect. Dis. 17*, 1472−1474.
(28) World Health Organization (2011) Global monitoring of antiviral resistance in currently circulating human viruses. *Weekly Epidemiological Record 86*, 497−508.
(29) van der Vries, E., Collins, P. J., Vachieri, S. G., Xiong, X., Liu, J., Walker, P. A., Haire, L. F., Hay, A. J., Schutten, M., Osterhaus, A. D., Martin, S. R., Boucher, C. A., Skehel, J. J., and Gamblin, S. J. (2012) H1N1 2009 pandemic influenza virus: Resistance of the I223R neuraminidase mutant explained by kinetic and structural analysis. *PLoS Pathog. 8*, e1002914.
(30) Vavricka, C. J., Li, Q., Wu, Y., Qi, J., Wang, M., Liu, Y., Gao, F., Liu, J., Feng, E., He, J., Wang, J., Liu, H., Jiang, H., and Gao, G. F. (2011) Structural and functional analysis of laninamivir and its octanoate prodrug reveals group specific mechanisms for influenza NA inhibition. *PLoS Pathog. 7*, e1002249.
(31) Wang, M. Z., Tai, C. Y., and Mendel, D. B. (2002) Mechanism by which mutations at His274 alter sensitivity of influenza A virus N1 neuraminidase to oseltamivir carboxylate and zanamivir. *Antimicrob. Agents Chemother. 46*, 3809−3816.
(32) Moscona, A. (2005) Oseltamivir resistance-disabling our influenza defenses. *N. Engl. J. Med. 353*, 2633−2636.
(33) Collins, P. J., Haire, L. F., Lin, Y. P., Liu, J., Russell, R. J., Walker, P. A., Skehel, J. J., Martin, S. R., Hay, A. J., and Gamblin, S. J. (2008) Crystal structures of oseltamivir-resistant influenza virus neuraminidase mutants. *Nature 453*, 1258−1261.
(34) Collins, P. J., Haire, L. F., Lin, Y. P., Liu, J., Russell, R. J., Walker, P. A., Martin, S. R., Daniels, R. S., Gregory, V., Skehel, J. J., Gamblin, S. J., and Hay, A. J. (2009) Structural basis for oseltamivir resistance of influenza viruses. *Vaccine 27*, 6317−6323.
(35) Wang, N. X., and Zheng, J. J. (2009) Computational studies of H5N1 influenza virus resistance to oseltamivir. *Protein Sci. 18*, 707−715.
(36) Ripoll, D. R., Khavrutskii, I. V., Chaudhury, S., Liu, J., Kuschner, R. A., Wallqvist, A., and Reifman, J. (2012) Quantitative predictions of binding free energy changes in drug-resistant influenza neuraminidase. *PLoS Comput. Biol. 8*, e1002665.
(37) Li, L., Li, Y., Zhang, L., and Hou, T. (2012) Theoretical studies on the susceptibility of oseltamivir against variants of 2009 A/H1N1 influenza neuraminidase. *J. Chem. Inf. Model. 52*, 2715−2729.
(38) Le, L., Lee, E. H., Hardy, D. J., Truong, T. N., and Schulten, K. (2010) Molecular dynamics simulations suggest that electrostatic funnel directs binding of tamiflu to influenza N1 neuraminidases. *PLoS Comput. Biol. 6*, e1000939.
(39) Woods, C. J., Malaisree, M., Long, B., McIntosh-Smith, S., and Mulholland, A. J. (2013) Computational Assay of H7N9 Influenza Neuraminidase Reveals R292K Mutation Reduces Drug Binding Affinity. *Science Reports*, manuscript submitted for publication.
(40) Frisch, M. J., et al. (2004) *Gaussian 03*, Gaussian, Inc., Wallingford, CT.
(41) Case, D., et al. (2012) *AMBER 12*, University of California, San Francisco.
(42) Li, H., Robertson, A. D., and Jensen, J. H. (2005) Very fast empirical prediction and rationalization of protein pKa values. *Proteins 61*, 704−721.
(43) Jorgensen, W. L., Chandrasekhar, J., Madura, J. D., Impey, R. W., and Klein, M. L. (1983) Comparison of simple potential functions for simulating liquid water. *J. Chem. Phys. 79*, 926−935.
(44) Duan, Y., Wu, C., Chowdhury, S., Lee, M. C., Xiong, G., Zhang, W., Yang, R., Cieplak, P., Luo, R., Lee, T., Caldwell, J., Wang, J., and Kollman, P. (2003) A point-charge force field for molecular mechanics simulations of proteins based on condensed-phase quantum mechanical calculations. *J. Comput. Chem. 24*, 1999−2012.
(45) Wang, J., Wolf, R. M., Caldwell, J. W., and Kollman, P. A. (2004) Development and testing of a general AMBER force field. *J. Comput. Chem. 25*, 1157−1174.
(46) Wang, J., Wang, W., Kollman, P. A., and Case, D. A. (2006) Automatic atom type and bond type perception in molecular mechanical calculations. *J. Mol. Graphics Modell. 25*, 247−260.
(47) Goetz, A. W., Williamson, M. J., Xu, D., Poole, D., Le Grand, S., and Walker, R. C. (2012) Routine microsecond molecular dynamics simulations with AMBER on GPUs. 1. Generalized Born. *J. Chem. Theory Comput. 8*, 1542−1555.

(48) Darden, T., Perera, L., Li, L., and Pedersen, L. (1999) New tricks for modelers from the crystallography toolkit: The particle mesh Ewald algorithm and its use in nucleic acid simulations. *Structure 7*, R55−R60.
(49) Ryckaert, J. P., Ciccotti, G., and Berendsen, H. J. C. (1997) Numerical integration of the cartesian equations of motion of a system with constraints: Molecular dynamics of n-alkanes. *J. Comput. Phys. 23*, 327−341.
(50) Seeber, M., Cecchini, M., Rao, F., Settanni, G., and Caflisch, A. (2007) Wordom: A program for efficient analysis of molecular dynamics simulations. *Bioinformatics 23*, 2625−2627.
(51) Humphrey, W., Dalke, A., and Schulten, K. (1996) VMD: Visual molecular dynamics. *J. Mol. Graphics 14*, 33−38.
(52) Baker, N. A., Sept, D., Joseph, S., Holst, M. J., and McCammon, J. A. (2001) Electrostatics of nanosystems: Application to microtubules and the ribosome. *Proc. Natl. Acad. Sci. U.S.A. 98*, 10037−10041.
(53) Baron, R., Setny, P., and Paesani, F. (2012) Water structure, dynamics, and spectral signatures: Changes upon model cavity-ligand recognition. *J. Phys. Chem. B 116*, 13774−13780.
(54) Baron, R., Setny, P., and McCammon, J. A. (2010) Water in cavity-ligand recognition. *J. Am. Chem. Soc. 132*, 12091−12097.
(55) Wang, L., Berne, B. J., and Friesner, R. A. (2011) Ligand binding to protein-binding pockets with wet and dry regions. *Proc. Natl. Acad. Sci. U.S.A. 108*, 1326−1330.
(56) Amaro, R. E., Minh, D. D., Cheng, L. S., Lindstrom, W. M., Jr., Olson, A. J., Lin, J. H., Li, W. W., and McCammon, J. A. (2007) Remarkable loop flexibility in avian influenza N1 and its implications for antiviral drug design. *J. Am. Chem. Soc. 129*, 7764−7765.
(57) Amaro, R. E., Cheng, X., Ivanov, I., Xu, D., and McCammon, J. A. (2009) Characterizing loop dynamics and ligand recognition in human- and avian-type influenza neuraminidases via generalized Born molecular dynamics and end-point free energy calculations. *J. Am. Chem. Soc. 131*, 4702−4709.
(58) Amaro, R. E., Swift, R. V., Votapka, L., Li, W. W., Walker, R. C., and Bush, R. M. (2011) Mechanism of 150-cavity formation in influenza neuraminidase. *Nat. Commun. 12*, 388.
(59) Woods, C. J., Malaisree, M., Hannongbua, S., and Mulholland, A. J. (2011) A water-swap reaction coordinate for the calculation of absolute protein-ligand binding free energies. *J. Chem. Phys. 134*, 054114.